Doig, Barber, et. al. Published in The Aeronautical Journal, 116(1178), April 2012. 407-430.

Aerodynamics of an aerofoil in transonic ground effect: numerical study at full-scale Reynolds numbers

G. Doig **T. J. Barber**
g.doig@unsw.edu.au
School of Mechanical and Manufacturing Engineering
The University of New South Wales
Sydney, Australia

A. J. Neely
School of Aerospace, Civil and Mechanical Engineering
The University of New South Wales at the Australian Defence Force Academy
Canberra, Australia

D. D. Myre
Aerospace Engineering Department
The United States Naval Academy
Maryland, USA

ABSTRACT

The potential positive effects of ground proximity on the aerodynamic performance of a wing or aerofoil have long been established, but at transonic speeds the formation of shock waves between the body and the ground plane would have significant consequences. A numerical study of the aerodynamics of an RAE2822 aerofoil section in ground effect flight was conducted at freestream Mach numbers from 0·5 to 0·9, at a range of ground clearances and angles of incidence. It was found that in general the aerofoil's lifting capability was still improved with decreasing ground clearance up until the point at which a lower surface shock wave formed (most commonly at the lowest clearances). The critical Mach number for the section was reached considerably earlier in ground effect than it would be in freestream, and the buffet boundary was therefore also reached at an earlier stage. The flowfields observed were relatively sensitive to changes in any given variable, and the lower surface shock had a destabilising effect on the pitching characteristics of the wing, indicating that sudden changes in both altitude and attitude would be experienced during sustained transonic flight close to the ground plane. Since ground proximity hastens the lower surface shock formation, no gain in aerodynamic efficiency can be gained by flying in ground effect once that shock is present.

NOMENCLATURE

α	angle of incidence
c	chord
C_L	co-efficient of lift
C_D	co-efficient of drag
C_f	co-efficient of skin friction
C_P	co-efficient of pressure
D	drag force
h	minimum height above ground plane
L	negative lift force (downforce)
M	local Mach number
M_∞	freestream Mach number
V_∞	freestream velocity
x	distance from leading edge

1.0 INTRODUCTION

Traditionally, aeronautical ground effect research (excluding study of vertical take-off and landing (VTOL)) has concentrated on the properties of wings in incompressible flows at relatively low subsonic Mach numbers. Applications have included aircraft in landing or takeoff modes or aircraft designed specifically to fly in ground effect (Wing-in-ground-effect, or WIG vehicles). In these cases, proximity to the ground serves to enhance the lifting performance of the wing, and often the aerodynamic efficiency (lift/drag, L/D) as well[1-3]. The principal effect of the ground is to move the stagnation point downwards as the wing experiences a reduction in velocity and an increase in pressure on the lower surface, accompanied by an increase in local velocity at the upper surface

Figure 1. A US Navy Blue Angel demonstration aircraft during a Mach 0·95 pass, highlighting shock/surface interaction (with permission: Matt Niesen).

suction peak near the leading edge[1,2]. This increases the effective angle of attach of the wing and lift as a consequence. Depending on the geometry, the ground effect can have a relatively small effect on drag. Therefore, the overall efficiency (L/D) of the wing can be greatly improved as ground clearance is decreased.

A much-improved understanding of the aerodynamic influence of compressible ground effects and of shock/ground interaction is timely, particularly given recurring interest in high-speed subsonic (freestream Mach number, $M_\infty \geq 0{\cdot}4$) WIG aircraft[3], as well as magnetic-levitation space vehicle launch systems[4], and high speed rail vehicles increasingly pushing towards the mid-subsonic Mach number range[5]. An example of shock/ground (in this case, water) interaction is shown in Fig. 1, where a US Navy Blue Angel performs an extremely low-level pass in San Francisco and generates a series of shockwaves, some of which influence the water surface.

In an extensive review of WIG aircraft aerodynamics and technology, Rozhdestvensky affirms 'it can be stated that little is still known with regard to GE (ground effect) at high subsonic Mach numbers'[6]. Brief test studies indicate that increased aerodynamic efficiency may be possible for a high aspect ratio wing in ground effect at high subsonic Mach numbers[7], but some simple analytical treatments suggest the opposite[6]. However, the effect of the formation of shock waves either on the wing upper surface, or between the wing and the ground, has not been considered in detail.

Other analytical studies using boundary element methods which considered subsonic and supersonic compressible flow over aerofoils in ground effect were limited by formulations can only be generally applied to thin aerofoils[8,9]. Despite this, results were presented for a (relatively thick) NACA 4412 aerofoil at 0° incidence, indicating that for a freestream Mach number of 0·5, the compressible case predicts C_L as being 12% higher for ground clearances greater than a height-to-chord ratio (h/c) of 0·5, below which the compressible C_L increasingly agrees with the incompressible prediction. No discussion was offered as to why this occurs and the method does not facilitate a detailed examination of the flowfield.

The present study applies RANS modelling to the situation of a two-dimensional aerofoil in ground effect at Mach numbers from 0·5 up to 0·9. The inclusion of a comprehensive set of experimental results for wings and aerofoils in transonic flowfields in the Advisory Group for Aeronautical Research and Development (AGARD) report of the late 1970s which was specifically compiled to provide numerical researchers with a validation database[10], has led the RAE2822 to become a common benchmark for transonic aerodynamic simulations. The decision was made to make use of this geometry not just because of the obvious possibility for validation of the numerical methods employed, but in order to enable the recontextualisation of this well-known aerofoil, such that its changed characteristics when in ground effect would stand in contrast to their 'freeflight' traits familiar to any researcher who has undertaken transonic aerofoil code validation. The present study included angle of incidence, Mach number (and by inference Reynolds number) and ground clearance as variables. Although the shape and camber of the body are clearly also important variables, adding these influences would have resulted in a prohibitive amount of data. Relevant parameters for the aerofoil in ground proximity are shown in Fig. 2.

2.0 NUMERICAL METHOD

The numerical method applied to produce all results in this section is very similar to that described in detail the accompanying part to this paper, 'Methods for blowdown wind-tunnel scale testing'[11], only differing in that in this instance it was applied to a purely two-dimensional geometry. In order to ensure the method established for conducting three-dimensional numerical analysis of the US Naval Academy wind-tunnel experiments was also sufficiently applicable to

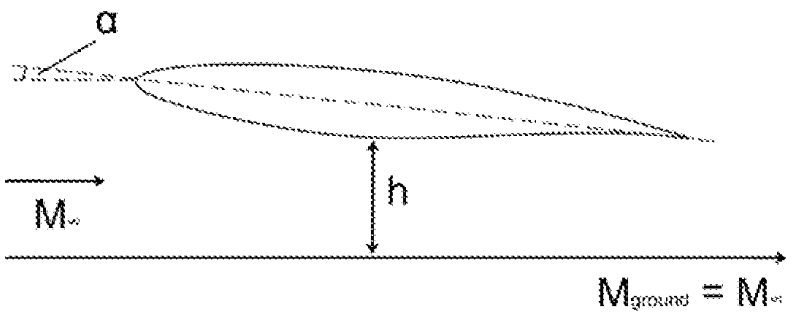

Figure 2. Parameters for an aerofoil in ground effect.

the present cases, additional validation was undertaken using the two-dimensional RAE2822 with reference to the AGARD report previously mentioned[10].

A commercial finite-volume Reynolds-Averaged Navier Stokes code, Fluent 6·3[12], was used to generate the results. A pressure-based, coupled solver was applied to obtain flow solutions, and convergence criteria were deemed to be met not only when the mass and momentum scaled-residual errors ceased to change by more than approximately 0·01% over 1,000 continued iterations, but also when the aerodynamic forces on the body ceased to change by more than 0·01% over 1,000 further iterations (for the steady-state simulations). All cases were run in 64-bit double precision using a second order node-based upwind discretisation scheme, and a standard three-coefficient Sutherland viscosity model was applied[13]. The choice of the pressure-based solver over the available density-based solver is discussed at the end of this section.

2.1 AGARD 'Case 9' comparisons

The AGARD 'Case 9' (a freestream Mach number of 0·73 and a corrected angle of incidence of 2·79°[10]) involves a strong normal shock wave sitting on the upper surface at approximately x/c = 0·53. The boundary layer behind the shock does not separate, allowing the flowfield to be effectively treated as stable and steady-state. The report indicates that a transition trip was located at x/c = 0·03, and the turbulent intensity of the oncoming flow was determined to be 0·1%. Both of these features were reproduced in the comparison simulations. The RAE 2822 section, at an aspect ratio of three and chord of 0·61m (in conditions yielding a Reynolds number of approximately $6{\cdot}5 \times 10^6$), was designed to provide two-dimensional flow at the semi-span. It has since been shown that this aspect ratio is not necessarily sufficient to ensure two-dimensional flow[14,15], and the results were influenced by the tunnel walls. Slotted walls were used to treat the boundary layers there; not only is little detail given about this in the original report, but this presents a scenario difficult to replicate in CFD.

Due to the wall influence, flow conditions for two-dimensional simulations are routinely corrected, sometimes by fixing the solution values for C_L and letting the solution find its own freestream conditions, or by adjusting either the Mach number or angle of incidence manually to match the experimental pressure distribution. The latter approach has been used here based on the suggestions of Cook *et al*[10]. The value of α used, 2·79°, is considerably altered from the experimental value of 3·19°. As is common practice, the tunnel walls are not considered, and the aerofoil is therefore treated as existing in free, unbounded flight.

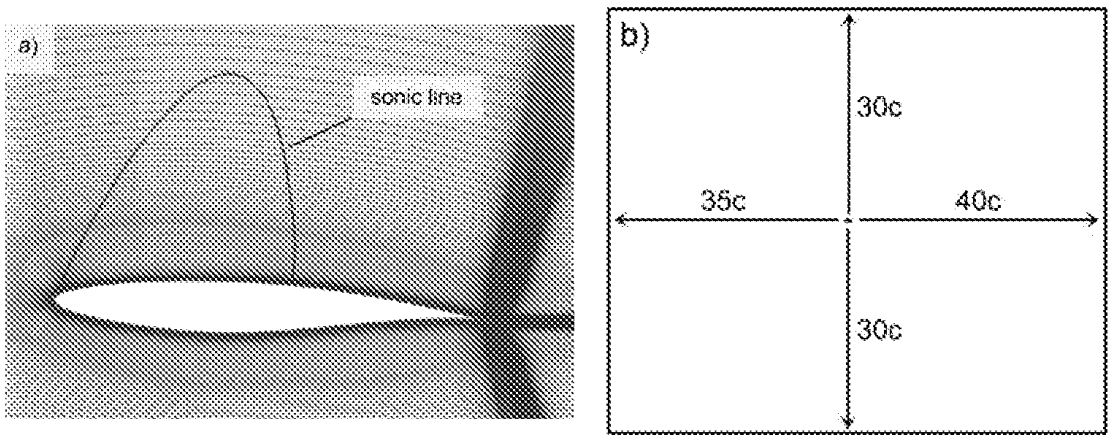

(a) (b)

Figure 3. Sample mesh (a) and domain extent (b) for RAE 2822 'Case 9' simulations.

2.2 Mesh and boundary considerations

The results presented in this section were generated by the Spalart-Allmaras turbulence model, the choice of which is discussed in the following section. All meshes were structured multi-block grids, the general layout of which can be seen in Fig. 3(a). The appropriate location for the farfield boundaries was examined simply by comparing the results from one simulation with boundaries as shown in Fig. 3(b), to those with an addition ten chord lengths in the domain in all directions. The influence of the boundaries on the solution when placed this far from the wings proved to be negligible, resulting in a changed prediction of the aerodynamic coefficients of less than 0·01%.

To ensure a mesh-independent solution, coarse, standard and fine meshes were constructed for evaluation. Local hanging-node refinement of the mesh at the shock location was also performed on the standard mesh. The coarse mesh contained 320 nodes on the wing surface and a total of 130,000 cells. The standard mesh contained 256,000 cells with 545 nodes on the wing. The fine mesh was simply the standard mesh with each cell quartered, and thus contained a little over 1 million cells. The initial comparison to the experimental pressure distribution, presented in Fig. 4, shows excellent agreement for all meshes. The shock location is well-predicted, at

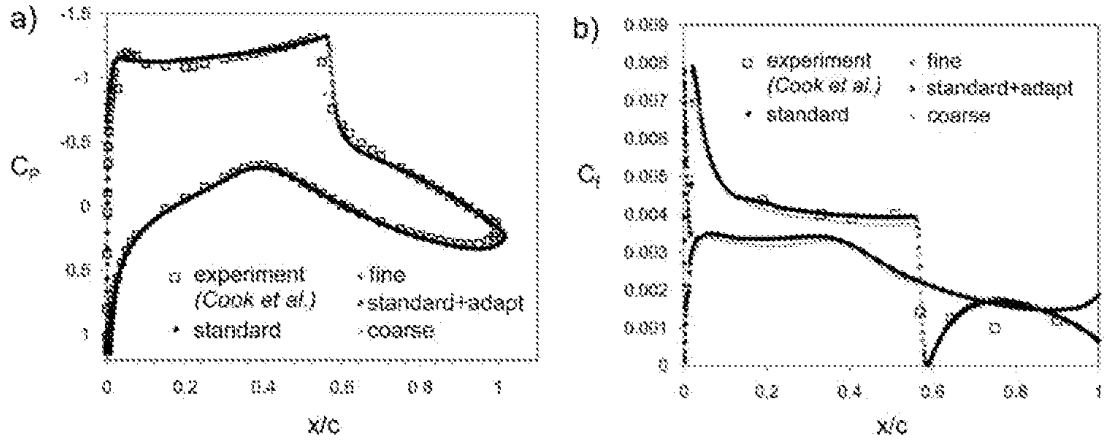

(a) (b)

Figure 4. Predicted pressure distributions for coarse, standard and fine meshes.

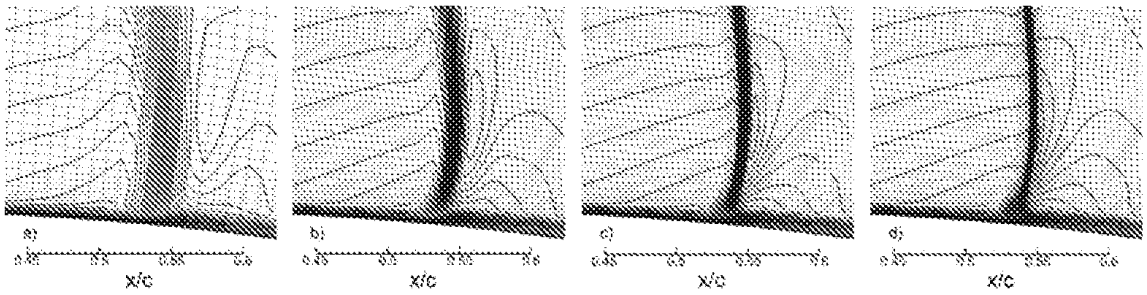

Figure 5. Resolution of density contours at the shock within the mesh for increasingly-refined node-spacing; a) coarse mesh, b) standard mesh, c) standard mesh first adaption, d) standard mesh with a second adaption.

around $x/c = 0{\cdot}54$, and although the shock strength is slightly overestimated and the pressure recovery exaggerated in the region immediately behind it, agreement to the trailing edge is generally good. Figure 4(a) indicates that the coarse mesh slightly underestimates the skin friction coefficient on the upper surface over the fore half of the aerofoil, but all meshes perform very similarly at and downstream of the shock.

A qualitative assessment of these meshes in the shock region is presented in Fig. 5. Although the mesh resolution does not have a marked influence on the actual location of the shock, the smearing of the contours in the coarse and standard meshes is notable. Local refinement of the mesh around the shock achieves a similar or even better resolution of the shock as seen with the fine mesh, albeit with only a few thousand additional cells, and thus was adopted as the preferred method in order to better capture the more complicated shock structures, including reflections, seen in the ground effect study.

Comparisons to the experimental lift and drag values are presented in Table 1. The experimental results do not incorporate a measure of error, but nevertheless the simulations provide a good match, with only the coarse mesh failing to achieve adequate drag predictions. There is essentially little to choose between the other meshes, and it is noted that while lift is within 1 to 2% of the experimentally-obtained value, drag is over-predicted in all cases and thus that feature is independent of the mesh density.

Table 1
Predicted lift (a) and drag (b) coefficients for different meshes

	Experiment	coarse	standard	fine	standard+adapt
C_L	0·803	0·791	0·789	0·789	0·789
C_D	0·0168	0·0142	0·0177	0·0177	0·0177

2.3 Turbulence modelling

The Spalart-Allmaras (SA)[16], Realisable k-ε[17], and k-ω SST[18] turbulence models were evaluated for their effectiveness in capturing the flowfield accurately. In the comparisons to experiment, transition was retained at $x/c = 0{\cdot}03$. However, a case was also run without transition (fully-turbulent) and, as seen in Fig. 6(a), very little observable difference in shock location and strength was observed. As this difference was so minor, the simulations in the main body of the ground effect study were thus run as fully turbulent as there was no reliable free-transition comparison data for such a wide range of shock behaviour in ground effect, and imposing one or more arbitrary transition locations would have introduced an additional influential variable.

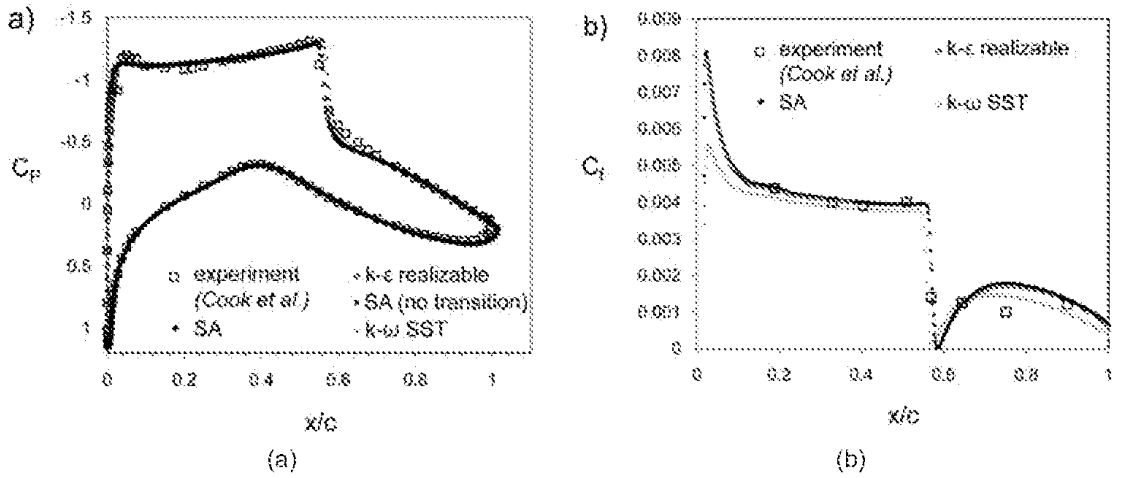

Figure 6. (a) Predicted pressure coefficients for two turbulence models with and without forced transition at 0·03c, and (b) predicted skin friction coefficients with forced transition (upper surface only).

The pressure distributions for all models in Fig. 6(a) show relatively minor differences between the predictions of the turbulence models, with the SA and Realisable models proving to be marginally closer to the experimental readings in the region of the shock. The SA model is also closest in reproducing the experimental lift coefficient, as shown in Table 2, although drag is still somewhat over-predicted. The case involving fixed transition actually features increased drag due to the slightly enhanced strength of the shock wave and the small increase to boundary layer thickness. The results indicate that the model will most accurately reproduce the experiment with the Spalart-Allmaras model when the transition is considered, but a fully-turbulent assumption is generally a very good approximation of the flow. This is particularly true for the parametric study which follows, where it is not necessary to consider transition as a variable in order to compare the results. Comparisons to skin-friction coefficients in the vicinity of the shock indicate that the SA turbulence model chosen has been shown to adequately capture the nature of the shock/boundary layer interaction in the validation case, as further demonstrated in literature[16,19]. Its performance is near-identical to that of the Realisable model, with the SST prediction slightly under-estimating the C_f over the region of the upper surface forward of the shock.

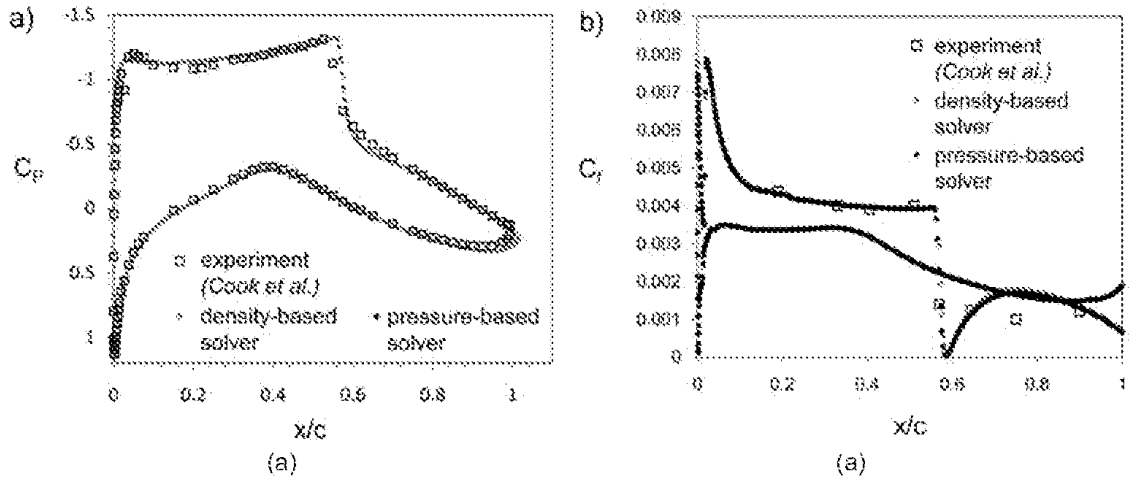

Figure 7. Predicted pressure coefficients for the pressure-based and density-based solvers for forced transition at 0.03c, and b) predicted skin friction coefficients with forced transition.

Returning to the choice of solver, comparisons to the reference experiments were made for results generated by the coupled pressure-based solver already described, and the explicit density-based solver also available in Fluent. Figure 7 indicates an essentially negligible difference in results for predicted pressure and skin friction coefficients, however the pressure-based solver was able to achieve satisfactory convergence in fewer than half the iterations. It also provided a more stable flowfield in the early stages of solution, particularly as the shock wave was established, and for all these reasons was deemed to be an appropriate and preferable solver for the study described in this manuscript.

Table 2
Predicted lift (a) and drag (b) coefficients for different turbulence models

	Experiment	Turb. SA	Transition SA	Turb. Realisable k-ε	Turb. k-ω SST
C_L	0·803	0·789	0·800	0·768	0·770
C_D	0·0168	0·0177	0·0180	0·0182	0·0163

3.0 RESULTS AND DISCUSSION

Initially, results for AGARD 'Case 9' conditions were re-examined for various ground clearances to provide an introductory comparison of cases for increasing ground proximity. Subsequent to this section, the full range of results for all variables is presented in terms of aerodynamic coefficients for two contexts: decreasing ground clearance for a fixed Mach number (analogous to reducing altitude at a controlled speed in a situation similar to that in Fig. 1), and increasing Mach number for a fixed ground clearance (acceleration of an aircraft at a fixed altitude more akin to what a wing-in-ground effect aircraft would experience).

3.1 'Case 9' with decreasing ground clearance

Here, the ground clearance is the only variable considered, in order to provide a clear indication of the effect on aerodynamic performance of increasing ground proximity as compared to the freeflight condition. The Reynolds number and scale remain the same as in the previous section; $6{\cdot}2 \times 10^6$ and a chord of 0·61m, respectively. As outlined in the previous section, the flowfield was treated as fully-turbulent for all cases.

Figure 8 illustrates the way in which the pressure distribution around the aerofoil changes as the ground clearance is reduced in stages. Several points of note are immediately apparent. Most importantly, the upper surface shock location moves progressively upstream from its freestream location, by about 25% of the chord by $h/c = 0{\cdot}1$. It also gradually reduces in intensity, resulting in a less severe pressure increase across the wave. One of the main reasons for this behaviour is the downward movement of the stagnation point at the leading edge, which also increases the strength of the suction peak near the leading edge on the upper surface. This increase in the effective angle of incidence draws the shock upstream, and creates a stronger adverse pressure gradient across the forward portion of the upper surface leading to the earlier, weaker shock and a reduction in the region of 'rooftop' pressure distribution. The flow remains attached at the foot of the shock.

At the same time, the pressure distribution on the lower surface of the aerofoil is affected as the air which is forced underneath is increasingly constricted by reducing ground

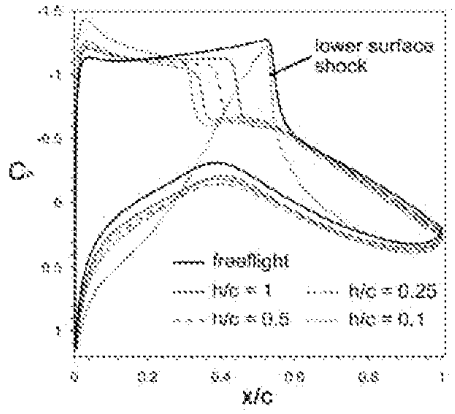

Figure 8. Pressure distribution for decreasing ground clearance at 'Case 9' conditions.

clearance. As more mass is directed over the upper surface, the lower velocity under the aerofoil causes higher pressure in the region between the aerofoil and the ground, particularly near the leading edge as the stagnation point is drawn downwards, and thus the maximum pressure difference between the upper and lower surface is exaggerated with increasing proximity to the ground.

These general trends hold until the lowest ground clearance, $h/c = 0{\cdot}1$. In this case, the flow between the aerofoil and the ground has accelerated to supersonic local Mach numbers, causing a strong shock wave at approximately $x/c = 0{\cdot}54$ as noted in Fig. 8. The lower surface Mach number local peak of approximately $M_l = 1{\cdot}36$ occurs immediately prior to the shock

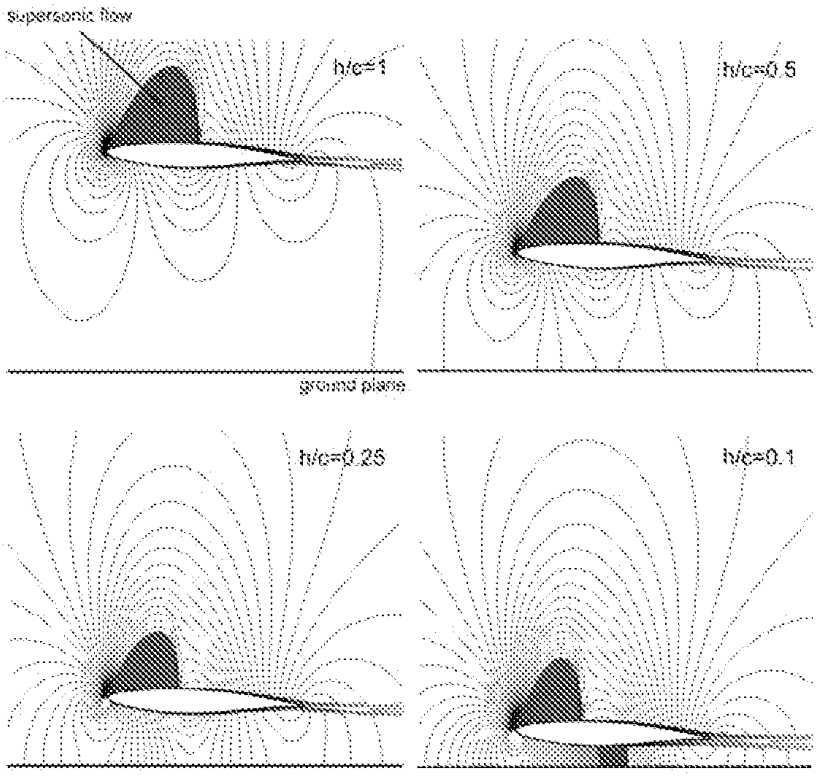

Figure 9. Contours of density and regions of supersonic flow around the aerofoil at Case 9 conditions as ground clearance is reduced from $h/c = 1$ to $0{\cdot}1$.

wave and the strength of the shock is such that it separates the flow from the surface in a small bubble. As a result, the lower surface boundary layer is considerably thickened to the trailing edge, and results in a broader wake boundary than at higher clearances. The forward movement and weakening of the upper shock as ground clearance is reduced, and then the emergence of the lower shock and thicker wake, are depicted in Fig. 9.

The influence of these effects on the lift and drag coefficients is shown in Fig. 10(a). Drag decreases with ground clearance until $h/c = 0{\cdot}1$ is reached. In subsonic cases, aerofoils with attached flow tend to experience a small reduction in pressure drag as the suction over the forebody of the wing can have a component which pulls the wing forwards to a small extent. The effect seen in the present cases is related, though the large (> 25%) reduction in drag is attributable to a much greater extent to the reduction in the strength of the shock wave, which diminishes the wave drag and lessens the thickening effect the shock has on the boundary layer (although this latter contribution to overall drag is much smaller). At $h/c = 0{\cdot}1$, the drag coefficient increases markedly, due to the emergence of the lower surface shock and the separated flow it produces.

C_L increases slightly from the freestream value, up 2% to $h/c = 0{\cdot}5$ and peaking at 5% higher at $h/c = 0{\cdot}25$. This is due to the increase of effective angle of incidence caused by increasing ground proximity, and the greater build up of higher pressure already noted between the aerofoil and the ground on the foremost portion of the aerofoil, which increases the maximum suction the section produces. The formation of the lower shock at $h/c = 0{\cdot}1$ destroys much of this capacity to create lift, as the flow is greatly accelerated under the aerofoil and produces a large amount of low pressure prior to the shock on the aft portion of the wing. This creates very strong gradients over the entirety of the chord on the lower surface. The relatively high curvature of this particular aerofoil section is a major contributor to this.

Figure 10(b) illustrates the changes to the aerofoil pitching moment (taken around the aerofoil ¼ chord) while the flowfields described above are developing. The presence of the ground serves to lessen the magnitude of the nose-down moment by between 10% and 15% at $h/c = 0{\cdot}5$ and 025 respectively, though this trend is not severe until $h/c = 0{\cdot}1$ is reached,

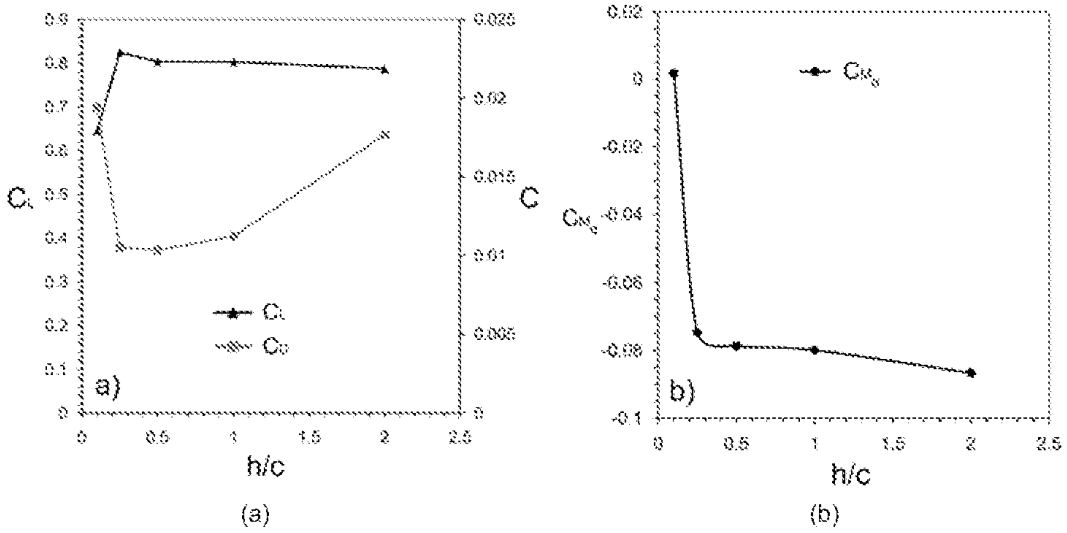

Figure 10. Lift and drag coefficients (a) and pitching moment coefficient (b) at Case 9 conditions as ground clearance is reduced from $h/c = 1$ to 0·1.

at which point the moment becomes a nose-up pitching tendency, as the lower surface shock forms behind the ¼ chord point and the strength of the upper surface suction diminishes.

Were the results for 'Case 9' in ground effect to hold across a range of Mach numbers and angles of incidence, the aerodynamics of the aerofoil in the mid-to-high subsonic regime would be fairly predictable. However, as will now be discussed, the flows can be very sensitive to changes in any variable. The RAE 2822 aerofoil was used for a broad, parametric study across several ground clearances (freeflight (no ground), and h/c = 1, 0·5, 0·25, and 0·1), Mach numbers (0·5, 0·6, 0·7, 0·8, 0·9) and angles of incidence (0°, 2·79° and 6°) as outlined in Table 3. Higher angles of incidence would be virtually impossible to achieve in ground effect while maintaining ground clearance at a stable cruise speed, as the additional lift would pull the body away from the ground plane. Higher freestream Mach numbers than 0·9 were not examined for the two-dimensional geometry in this case, as the inability of the flow to relax in the third dimension would eventually lead to rather unrealistic detached bow shock waves at freestream Mach numbers far lower than that at which they could be expected to appear for any real-world body bar one with very high aspect ratio wings.

The results presented from this point onwards use an aerofoil which is scaled to be 5 times greater than that of the 'Case 9' tests, to better approximate real world flight Reynolds numbers. Thus the chord is 3·05m, and the chord-based Reynolds numbers for each Mach number considered are as outlined in Table 3. The case matrix of all simulations is presented in Table 4, and highlights which cases were run as steady-state, which were run as transient but which came to a steady-state with the relaxation in time, and those which featured transient regular oscillatory shock motion. Any aerodynamic force coefficients and pressure distributions presented for the latter type are time-averaged over three oscillation cycles in subsequent diagrams. For the sake of brevity a full analysis of the transient cases is not presented here, however it is worth noting that: cases featuring regular oscillatory behaviour were unambiguously unsteady from early stages of the simulation, requiring timesteps of the order of 0·001s to produce regular behaviour satisfactorily; simulations which showed very mild unsteadiness generally stabilised to a steady state with a similar or smaller timestep, indicating that the instability was more of a numerical artefact than genuine behaviour.

Table 4 also allows the reader to see at a cursory glance which flowfields included areas of supersonic flow, and therefore in broad terms the reduction of critical Mach number with decreasing ground clearance for certain conditions is revealed. It is also worth noting that there is no clear pattern when it comes to the onset of unsteady shock behaviour as indicated by the transient cases, and as such these results hint that the buffet boundary of the aerofoil, in addition to the other more familiar variables, may be highly sensitive to ground clearance.

Table 3
List of Mach numbers and related parameters

M_∞	U_∞(ms^{-1})	Reynolds Number
0·5	170·04	$35{\cdot}52 \times 10^6$
0·6	204·05	$42{\cdot}63 \times 10^6$
0·7	238·05	$49{\cdot}73 \times 10^6$
0·8	272·06	$56{\cdot}84 \times 10^6$
0·9	306·07	$63{\cdot}94 \times 10^6$

Table 4
List of simulations conducted, detailing which cases were run as fully transient (marked Unsteady), which transient solutions tended to a steady state (*U-S*) and which featured areas of supersonic flow around the aerofoil ($M_l > 1$)

$h/c = \infty$ (Freeflight)	$\alpha = 0°$	$\alpha = 2{\cdot}79°$	$\alpha = 6°$
$M_\infty = 0{\cdot}5$	$M_l < 1$	$M_l < 1$	$M_l > 1$
0·6	$M_l < 1$	$M_l > 1$	$M_l > 1$
0·7	$M_l < 1$	$M_l > 1$	Unsteady
0·8	$M_l > 1$	$M_l > 1$	$U - S$
0·9	$M_l > 1$	$M_l > 1$	$M_l > 1$
$h/c = 1$	**$\alpha = 0°$**	**$\alpha = 2{\cdot}79°$**	**$\alpha = 6°$**
$M_\infty = 0{\cdot}5$	$M_l < 1$	$M_l < 1$	$M_l > 1$
0·6	$M_l < 1$	$M_l > 1$	$M_l > 1$
0·7	$M_l < 1$	$M_l > 1$	$U - S$
0·8	$M_l > 1$	$U - S$	$U - S$
0·9	$M_l > 1$	$M_l > 1$	$M_l > 1$
$h/c = 0{\cdot}5$	**$\alpha = 0°$**	**$\alpha = 2{\cdot}79°$**	**$\alpha = 6°$**
$M_\infty = 0{\cdot}5$	$M_l < 1$	$M_l < 1$	$M_l > 1$
0·6	$M_l < 1$	$M_l < 1$	$M_l > 1$
0·7	$M_l < 1$	$M_l > 1$	$M_l > 1$
0·8	$M_l > 1$	$U - S$	$U - S$
0·9	$M_l > 1$	$M_l > 1$	$M_l > 1$
$h/c = 0{\cdot}25$	**$\alpha = 0°$**	**$\alpha = 2{\cdot}79°$**	**$\alpha = 6°$**
$M_\infty = 0{\cdot}5$	$M_l < 1$	$M_l < 1$	$M_l > 1$
0·6	$M_l < 1$	$M_l > 1$	$M_l > 1$
0·7	$M_l > 1$	$M_l > 1$	$U - S$
0·8	$U - S$	$U - S$	$U - S$
0·9	$M_l > 1$	$M_l > 1$	$M_l > 1$
$h/c = 0{\cdot}1$	**$\alpha = 0°$**	**$\alpha = 2{\cdot}79°$**	**$\alpha = 6°$**
$M_\infty = 0{\cdot}5$	$M_l > 1$	$M_l < 1$	U – S
0·6	Unsteady	$M_l > 1$	$M_l > 1$
0·7	$M_l > 1$	$M_l > 1$	$M_l > 1$
0·8	Unsteady	Unsteady	$U - S$
0·9	$M_l > 1$	$M_l > 1$	$M_l > 1$

3.2 Decreasing ground clearance for fixed Mach numbers

3.2.1 2·79° incidence

Of the three incidences examined in this section, 2·79° is most representative of an actual flight condition, as it is a lifting configuration that would be relatively low-drag, and is therefore discussed in most detail here. The angle of the section ensures that there is not as strong an

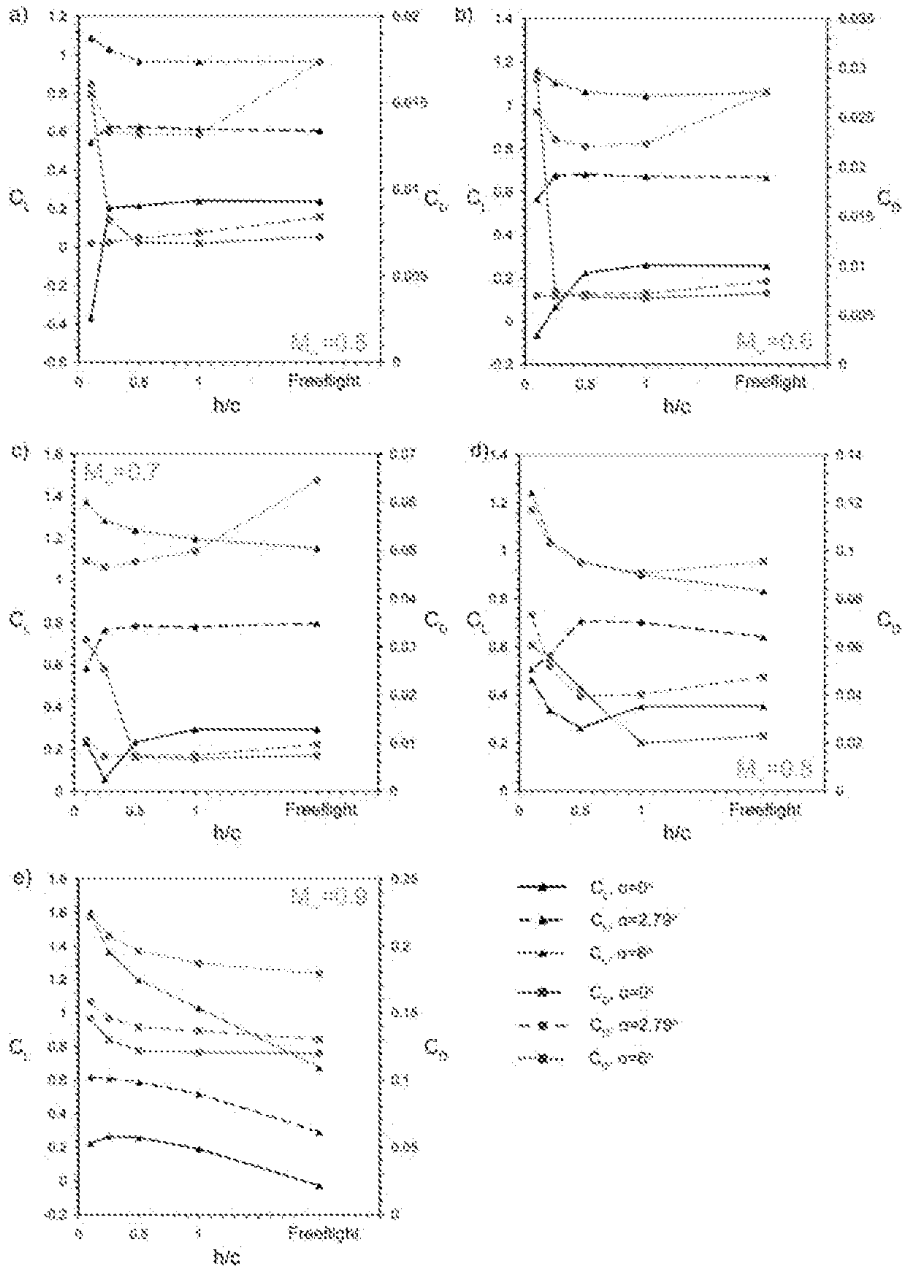

Figure 11. Lift and drag coefficients for 0°, 2·79° and 6°, with decreasing ground clearance for (a) $M_\infty = 0{\cdot}5$, (b) 0·6, (c) 0·7, (d) 0·8 and (e) 0·9.

acceleration of flow between the aerofoil and ground as at 0°, and there is not the strong tendency for separation on the upper surface as at 6°. Aerodynamic coefficients are presented in Fig. 11; aerodynamic efficiency is discussed in Section 3.3.

At $M_\infty = 0{\cdot}5$, C_D reduces by approximately 20% from freeflight to $h/c = 0{\cdot}1$, accompanied by a 14% increase in C_L from freeflight to $h/c = 0{\cdot}25$, after which there is a marked drop at $h/c = 0{\cdot}1$. The drag reduction stems from a diminishment of the slight downwash angle of the wake from the trailing edge, as the high pressure region near the lower trailing edge grows with decreasing clearance, and this also contributes to the overall lift of the section which benefits from a higher effective angle of incidence despite the mild changes to the wake angle. The drop

in lift at $h/c = 0{\cdot}1$ stems from a marked local acceleration of the flow around the lower surface through the area of minimum ground clearance, where the peak local Mach number is approximately 13% higher than the equivalent freeflight case. At higher clearances, this increased local Mach number effect is slight.

These trends remain largely unchanged at $M_\infty = 0{\cdot}6$, but now the lift-loss at $h/c = 0{\cdot}1$ is more pronounced. For cases at all the higher clearances, C_L is proportionally higher than at $M_\infty = 0{\cdot}5$, and C_D lower, as the effects described previously are enhanced. In all cases, a small region of supersonic flow has emerged around the upper surface, close to the leading edge. In freeflight, peak M_l is 1·03, and at $h/c = 0{\cdot}1$, M_l is 1.11.

At $M_\infty = 0{\cdot}7$, the trends again remain largely unchanged, despite all cases featuring an upper surface shock. Instead of a slight increase in lift, there is a 3% decrease from freeflight to $h/c = 0{\cdot}25$, though a drag reduction remains over the same range of ground clearances. We have already seen in the previous section, for the similar 'Case 9' conditions, that this is a result of the shock wave reducing in strength as it is drawn forward as the ground is approached, with the flow having a shorter region over which to accelerate before the terminating shock. The gain in lift made from an increased effective angle of incidence is countered by the shortened run of acceleration prior to the shock, which reduces the low pressure the aerofoil is able to generate there.

At $h/c = 0{\cdot}1$, there now exists a lower shock between the aerofoil and ground, and a significant accompanying drag rise is observed, along with a drop in lift due to the intense pressure drop underneath the section which is the culmination of the undersurface acceleration effect which had been building at this ground clearance from $M_\infty = 0{\cdot}5$.

By $M_\infty = 0{\cdot}8$, both $h/c = 0{\cdot}1$ and 0·25 feature lower shocks, explaining the sudden increase in drag and decrease in lift at these clearances. Further from the ground plane, the flow is now detached behind the upper shocks to the trailing edge, and results in a much stronger, thicker wake, and so C_D has risen an order of magnitude from the $M_\infty = 0{\cdot}7$ cases. It is clear that the closest ground clearances will affect the critical Mach number of the section; particularly that of the lower surface shock wave, which appears weakly around the aerofoil in freestream at a point close to $M_\infty = 0{\cdot}8$, whereas at the closest ground proximity it has been present on the wing since $M_\infty = 0{\cdot}6$. At clearances where the lower shock is not present, the efficiency of the wing remains improved by the ground influence.

At $M_\infty = 0{\cdot}9$, extremely large-scale shock structures exist at the trailing edge. The RAE 2822 section was designed for optimal effectiveness at sub-critical Mach numbers (design condition $M_\infty = 0{\cdot}66$ at $\alpha = 1{\cdot}06°$), and so at this upper range of the Mach number scale it features very poor aerodynamic performance. Additionally, the two-dimensional nature of these simulations is liable to produce exaggerated shock structures that would be unlikely to exist in three-dimensional cases up until freestream Mach numbers closer to the immediate vicinity of one. Nevertheless, the shock structures produced, particularly at the point of ground reflection, are worthy of inspection. In terms of the aerodynamic forces, it is sufficient to observe that the lift and drag trends are now clear and stable, as the both upper and lower shocks sit at the trailing edge in both cases.

Lift coefficient increases with decreasing clearance simply because the acceleration of the upper surface continues to be enhanced by the presence of the ground, and the lower surface shock for the ground effect cases at or below $h/c = 0{\cdot}5$ does not sit on the aerofoil itself; rather, in the supersonic flowfield, a series of weaker compression waves are generated by the trailing edge contour from $x/c = 0{\cdot}96$, and subsequently coalesce into a shock wave away from the aerofoil. Drag coefficient increases as well with decreasing ground clearance, as the strength of the shocks increase and therefore so does wave drag, and the complexity of their interaction

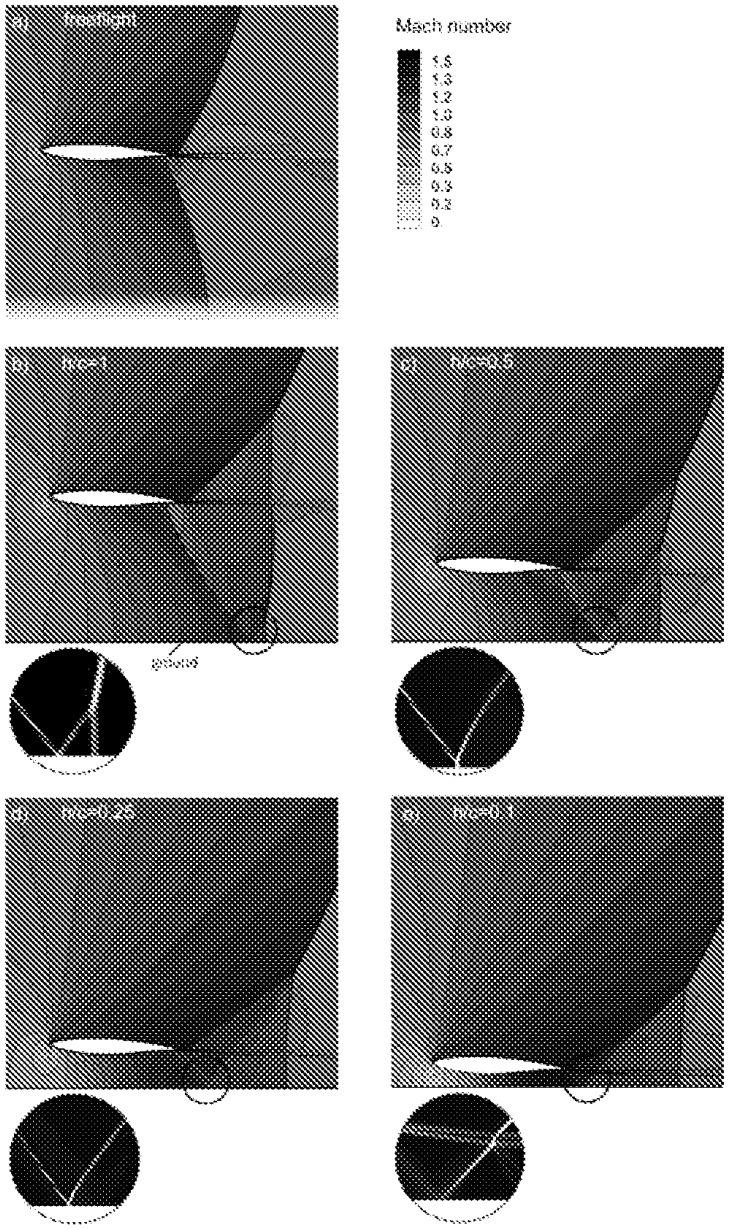

Figure 12. Contours of Mach number and (inset detail) numerical schlieren for cases at $M_\infty = 0{\cdot}9$, $\alpha = 2{\cdot}79^\circ$, as ground clearance is reduced from (a) freeflight, to (b) $h/c = 1$, (c) $h/c = 0{\cdot}5$, (d) $h/c = 0{\cdot}25$ and (e), $h/c = 0{\cdot}1$.

with the wake following reflection from the ground plane in all cases serves to thicken the free shear layers trailing the aerofoil.

A series of images illustrating these features is shown in Fig. 12 for the $M_\infty = 0{\cdot}9$ cases, along with numerical schlieren insets detailing the nature of the ground interactions. From freeflight to $h/c = 1$, the peak local Mach number prior to the upper shock increases from approximately 1·6 to 1·7, increasing the oblique angle of the shock in the wing vicinity. This effect is exaggerated with further proximity to the ground, as the extent of the high-Mach region increases. In all cases this oblique wave is observed to normalise in the far field, many chord lengths' from the aerofoil. At $h/c = 1$, the lower shock experiences regular reflection, which is

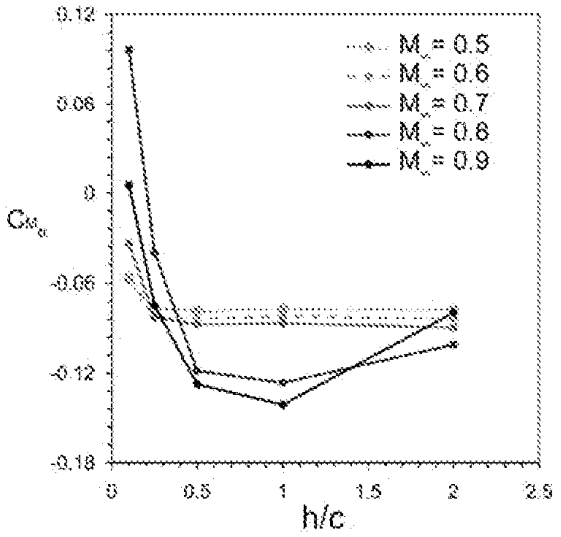

Figure 13. Pitching moment coefficients at $\alpha = 2.79^\circ$, as ground clearance is reduced.

followed by a normal recompression stem; these two waves join in forming a large normal recompression approximately 0·5*c* downstream from the trailing edge, bringing the flowfield back to a subsonic condition. The shock structure is highly reminiscent of that generated by the F/A 18 during the high-speed pass captured in the photograph of Fig. 1.

At the ground, a 'lambda' shock structure, different from that seen on the wing in the validation cases, forms in the presence of the thin shear layer which has formed on the ground. This flow feature is highlighted in the inset of Fig. 12(b), showing a triple-point forming at the meeting of the reflected incident shock and the Mach stem to the ground surface. The shear layer thickens behind this point.

At $h/c = 0{\cdot}5$, the general structure is identical, but the extent is magnified. The reflection at the ground, which now features its own small Mach stem due to the reduction in the angle of the incident shock (and therefore takes on a more conventional reflection structure[20]), is able to pass through the wake before being joined by the strong normal stem from the ground at close to 0·65*c* downstream of the trailing edge. The influence of this on the wake is to thicken it considerably, and align it with the freestream following a mild downwards deflection from the trailing edge. The major triple point sits above the wake, further from the ground than the aerofoil, representing a considerable evolution from the structure seen at $h/c = 1$.

By $h/c = 0{\cdot}25$ the immediate downwards deflection of the wake is more prominent and the reflected lower wave now passes through the wake and merges with the normal recompression and the upper shock at a unique quadruple point. The lower wave itself now no longer forms at the aerofoil surface; rather, a series of compression waves are generated due to the curvature of the lower surface close to the trailing edge. These waves coalesce into a shock at the ground plane, and therefore the reflection itself is weaker – the Mach number gradients in this region are not as pronounced as at the higher clearance.

The same is true of the wave at $h/c = 0{\cdot}1$, and the peak local Mach number in the flowfield now occurs at the ground plane immediately prior to the shock reflection. The upper wave now merges with the reflection of the lower wave prior to the normal recompression to subsonic conditions, which occurs 0·8(c) downstream of the trailing edge. The reflected lower wave straightens the wake to parallel with the freestream, but the numerical schlieren in the inset of Fig. 11(e) indicates that a weak reflection of the wave from the shear layer also exists, and the

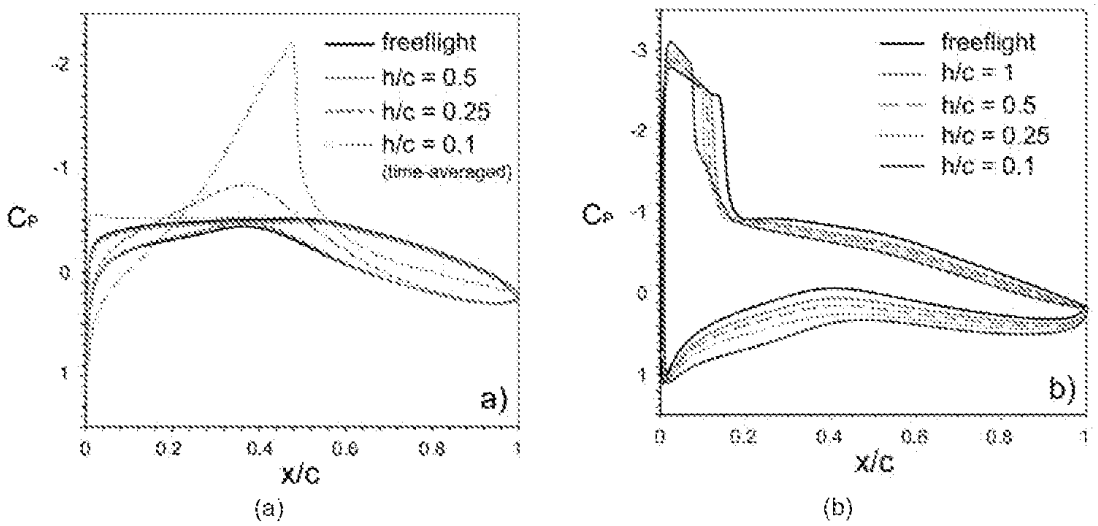

(a) (b)

Figure 14. Pressure distributions at M_∞ = 0·6 for (a) $\alpha = 0^\circ$ and (b) $\alpha = 6^\circ$ as ground clearance is reduced.

wave itself bends significantly in passing through the shear layers. However, its angle in exiting this region is essentially unchanged from that prior to the interaction.

Figure 13 presents a plot of pitching moment coefficient, taken around the ¼ chord mark, for $\alpha = 2{\cdot}79^\circ$, as ground clearance is reduced and for the five freestream Mach numbers investigated. At $M_\infty = 0{\cdot}5$ through 0·7, the nose-down moment is fairly constant with decreasing clearance, until $h/c = 0{\cdot}1$ is reached, at which point the moment becomes notably less negative due to the increase in low pressure forming between the aerofoil and the ground. This reaches its peak behind the ¼ chord and therefore contributes a nose-up (positive) component. At $M_\infty = 0{\cdot}8$, the negative moment increases in magnitude from freeflight to $h/c = 1$, after which it becomes considerably less negative with further reduction in ground clearance, eventually producing an overall nose-up moment at $h/c = 0{\cdot}1$, coinciding with the point where the lift coefficient was seen to drop away in Fig. 11.

3.2 0° incidence

Although not typical of a flight incidence except in momentary pitching, the 0° cases provide the most exaggerated ground effects due to the lower surface producing a relatively stronger venturi effect between the aerofoil and the ground.

Returning to Figure 11(a), for $M_\infty = 0{\cdot}5$, the lift coefficient is seen to decrease slightly as ground clearance is reduced. This is a direct consequence of the increasing acceleration of the flow between the aerofoil and ground, which is more exaggerated at this incidence than at 2·79°, and means that the stagnation point is drawn upwards by a small margin. At $h/c = 0{\cdot}1$, the lift coefficient reverses sign, and the section produces a negative C_L of –0·39, or roughly –200% of the lift produced at $h/c = 0{\cdot}25$. The drag coefficient initially reduces by a small margin (1-2%) to $h/c = 0{\cdot}5$, after which it increases sharply with further proximity to the ground. At $h/c = 0{\cdot}25$ this is simply a function of the accelerated flow around the wing causing a slightly thicker wake, but at $h/c = 0{\cdot}1$ a shock wave has formed on the lower surface. There is no significant separation at the foot of the shock but the wake is markedly thicker as a result of the shock/boundary layer interaction.

For $M_\infty = 0{\cdot}6$, in Fig. 11(b), the trends are almost identical apart from that the marked drop-off in lift and mild increase in drag at $h/c = 0{\cdot}25$ (where lift remains positive in sign), as well

as h/c = 0·1 where the lower surface shock is present (again producing negative lift). At h/c = 0·25 this new trend is caused by the increased acceleration of the flow under the wing, where the peak local Mach number now 0·85, as opposed to a peak of M_l = 0·73 on the lower surface in the freeflight case. The h/c = 0·1 lower surface shock, which has begun oscillating, has now triggered significant periodic boundary layer separation from the shock foot to the trailing edge, and is the cause of the exponential rise in C_D, close to 100% higher than at the same clearance at M_∞ = 0·5.

Although other cases feature shock oscillation (noted in Table 4), this case was the only one to produce mild buffet flow specifically with the lower shock, and therefore has been singled out as a brief example. The shock movement was limited to a 0·03c portion of the aerofoil, with a low oscillation frequency of 16Hz. The shock foot periodically separated the boundary layer to the trailing edge.

The evolution of the flow with decreasing ground clearance to produce this flowfield is highlighted in Fig. 14. Aerofoil pressure distributions show the relatively mild ground influence at h/c = 0·5, where the distribution is close to that of the freeflight case. At h/c = 0·25, the acceleration of flow in the aerofoil/ground channel lowers the pressure there, while the upper surface distribution remains similar. Then, at h/c = 0·1, the shock wave forms, causing a large low pressure spike on the lower surface. With the flow so restricted underneath the aerofoil, the air directed over the upper surface produces a greater suction peak close to the leading edge, though this is more than offset by the negative lift produced by the suction region prior to the shock.

At M_∞ = 0·7, a shock has now formed on the lower surface at h/c = 0·25 and at h/c = 0·1. The effective choking of the flow between the aerofoil and ground has forced sufficient air over the upper surface to result in near-sonic conditions there. The lower surface shock was not oscillating, indicating that the increased Mach number lies on the far side of the buffet boundary produced by this wave. The drag rise now begins at h/c = 0·25, though no significant separation exists from that shock.

For M_∞ = 0·8, in Fig. 11(d), the marked drag rise is now present at h/c = 0·5 too; the flowfield incorporates both an upper and lower surface shock system. At h/c = 0·1, the flowfield is significantly transient once more, as the upper surface shock is now oscillating, with the periodic separation structures at the trailing edge triggering a mild movement in the lower shock as well. C_L initially drops as ground clearance is reduced from h/c = 1 to 0·5, but then increases despite the presence of the shocks. The flow is being forced over the upper surface to an extent that the low pressure region there is much extended with decreasing clearance, though it does result in a stronger shock sitting further back on the aerofoil.

At M_∞ = 0·9, extremely large-scale shock structures exist at the trailing edge as in the previous section, although they are not sufficiently different enough from the 2·79° cases, in terms of general characteristics, to warrant a detailed description here.

3.3 6° incidence

Although the incidence here is high enough to promote large-scale separation on the upper surface, the flow between the aerofoil and ground is closer to the 'ram' effect that can be achieved at lower incidence for a more flat-bottomed aerofoil section[3], as the profile is fairly parallel with the ground from the point of minimum ground clearance to the trailing edge. In this scenario, the region under the aerofoil is almost exclusively a high pressure zone, and features relatively little local acceleration due to curvature.

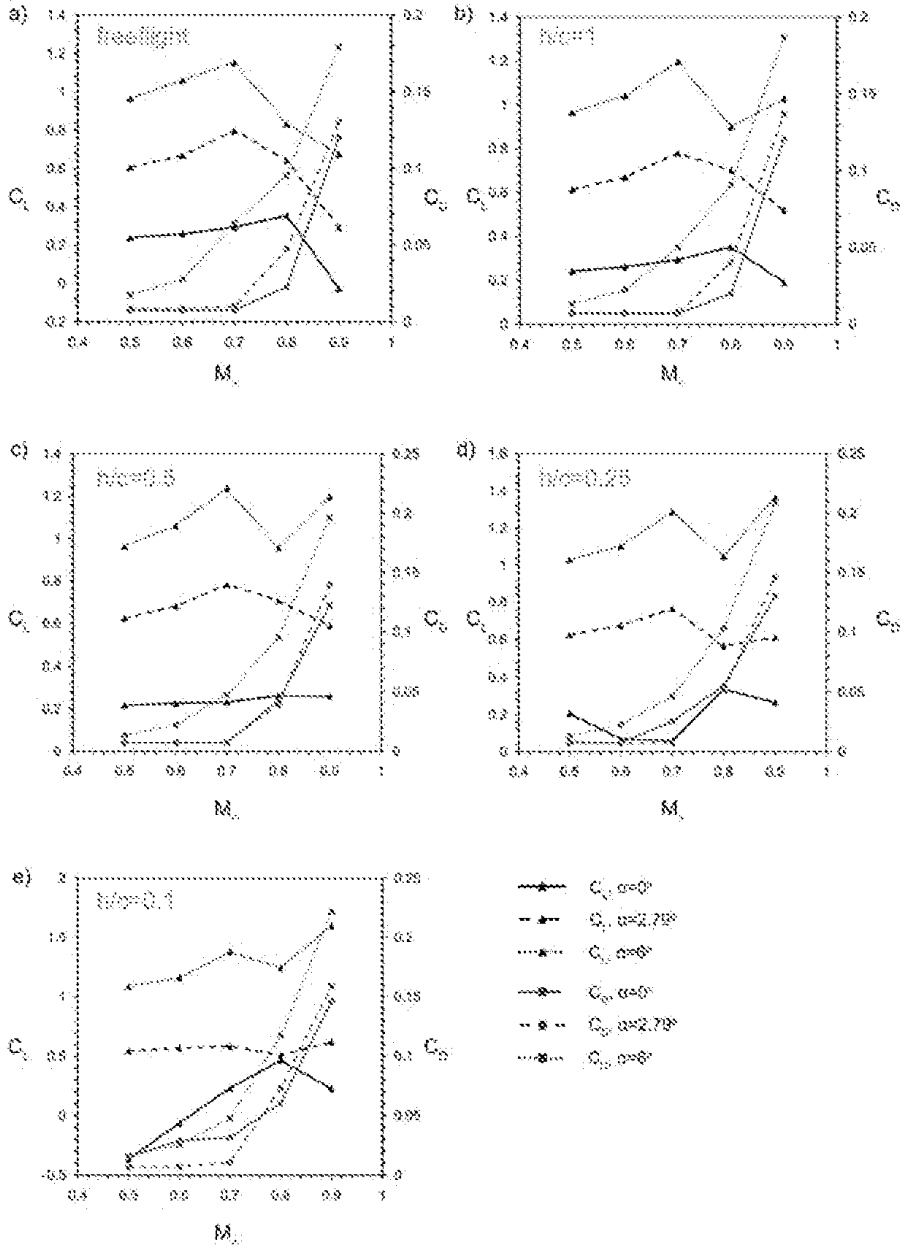

Figure 15. Lift and drag coefficients for 0°, 2·79° and 6°, with decreasing ground clearance for (a) M_∞ = 0·5, (b) 0·6, (c) 0·7, (d) 0·8 and (e) 0·9.

In the absence of lower surface shock waves up until $M_\infty = 0{\cdot}9$, most of the observed changes to lift and drag, referring back to Fig. 10, are due to the influence of the ground on the upper surface shock. At $M_\infty = 0{\cdot}5$ and 0·6, C_L only shows distinct improvement at $h/c = 0{\cdot}25$ and 0·1. Above this clearance, the 'ram' effect is not as strong. Prior to $h/c = 0{\cdot}1$, the drag reduces by almost 24% in ground effect as compared to the freeflight case, as the shock wave moves even further towards the leading edge, and the thickness of the upper shear layer leaving the aerofoil at the trailing edge is reduced as a result. The downwash angle of the wake is also lessened (1-2° in the immediate vicinity of the trailing edge). At the lowest clearance, lift and drag increase from their levels further from the ground. The drag increase is due to the fact that although the shock is even further forward on the profile as a result of the continued increase to effective angle

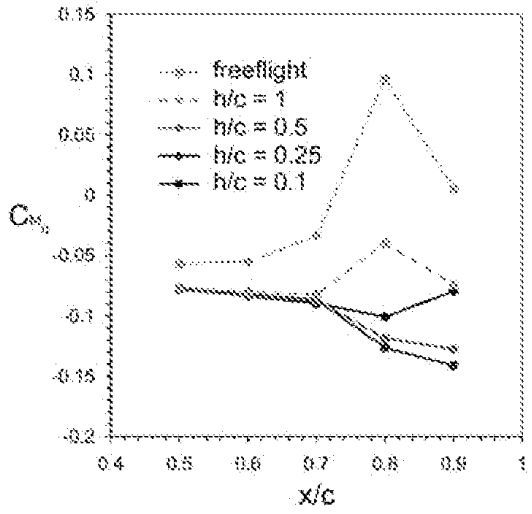

Figure 16. Pitching moment coefficients at $\alpha = 2{\cdot}79^{\circ}$, as Mach number increases.

of incidence, the flow is now significantly separated at the foot of the shock and therefore the boundary layer following reattachment downstream remains thicker and increases the strength of the wake as a result. Pressure coefficients with decreasing clearance for $M_{\infty} = 0{\cdot}6$ are shown in Fig. 14(b) to illustrate these effects.

These trends continue to hold at $M_{\infty} = 0{\cdot}7$, though the drag now increases across the range as separation bubbles at the shock foot are present in all the cases. The influence of the ground to this point appears to be to invoke the onset and subsequent magnification of separation by virtue of continued increase in the effective angle of incidence. However, the ability of the wing to produce ever-increasing levels of lift as clearance is reduced for a fixed Mach number is not affected. At $M_{\infty} = 0{\cdot}8$, with every case producing large areas of separated flow to the trailing edge, the 'ram' effect on the lower surface still results in increasing efficiency as the aerofoil is placed closer to the ground.

At M_{∞} 0·9, lift and drag both increase as ground clearance is reduced. In freeflight, the upper surface shock sits at the trailing edge, forming a lambda-foot with the upper shear layer behind the trailing edge, while a strong shock exists on the lower surface past the point of maximum thickness. After this compression, the lower surface flow accelerates to supersonic again, resulting in a second, much smaller, shock coincident with the stem of the upper shock.

At $h/c = 1$, the initial lower-surface shock has reduced greatly in magnitude, and the secondary region of supersonic flow is now much expanded, extending to the ground plane and forming a large-scale curved recompression shock. This structure does not change characteristics as clearance is further reduced, though the peak local Mach number prior to the upper shock increases and the final recompression behind the aerofoil exists increasingly downstream of the trailing edge as was seen for the 2·79° case. The elimination of the initial lower surface shock seen at higher clearances greatly increases the ability of the wing to produce lift.

3.4 Increasing Mach numbers for fixed ground clearances

For the three incidences examined, data is reconstructed in Fig. 15 for fixed angles of incidence and ground clearances as Mach number increases. This is briefly examined here as it is approximately representative of attempting flight at a constant attitude and altitude during long-term

acceleration, albeit at a slow enough rate so that the flow is steady-state at any given time. This provides a different way of interpreting the results. It ignores the intrinsic short-term effects of sudden acceleration, which would alter the results were this a truly time-dependent increase in freestream Mach number. Freeflight results are included for comparison.

3.4.1 0° incidence

In freeflight, lift and drag coefficients increase with Mach number, until at $M_\infty = 0{\cdot}9$ lift production drops off. At $h/c = 0{\cdot}5$, this drop is eliminated and lift coefficient remains largely constant through the Mach number range, though the drag increases at a greater magnitude. This clearance produces the most stable trends; at $h/c = 0{\cdot}25$, C_D at first decreases from M_∞ 0·5 to 0·6, then increases to M_∞ 0·8, then decreases again to M_∞ 0·9, due to the influence of the formation of the lower surface shock. The transonic drag rise begins between M_∞ 0·6 and M_∞ 0·7 as a result, rather than between M_∞ 0·7 and M_∞ 0·8 at the higher clearances. At $h/c =$ 0·1, as we have already seen, the wing produces negative lift until M_∞ 0·7, and as the lower surface shock has already formed prior to M_∞ 0·5, the transonic drag rise has already established itself.

3.4.2 2·79° incidence

With increased incidence, trends for lift and drag with increasing Mach number remain similar from freeflight to $h/c = 0{\cdot}5$, with the flowfields at M_∞ 0·7 representing a peak in the lift coefficient after which it drops off with the additional acceleration under the aerofoil to the point at which the lower shock forms. Drag rises predictably and asymptotically with Mach number for these cases and those at lower ground clearances as well. At $h/c = 0{\cdot}25$ and 0·1, C_l still peaks at M_∞ 0·7, then drops, but makes a partial recovery at M_∞ 0·9.

Pitching moment coefficient trends for this incidence are presented in Fig. 16, and show a clear distinction between the clearances from freeflight to $h/c = 0{\cdot}5$, and those at $h/c = 0{\cdot}25$ and 0·1. A spike in the CM_α at M_∞ 0·8 at these latter clearances is due to the marked shift forwards of the peak high pressure region, which now dominates the lower region close to the leading edge, rather than at the point of minimum clearance or the trailing edge where it is produced more

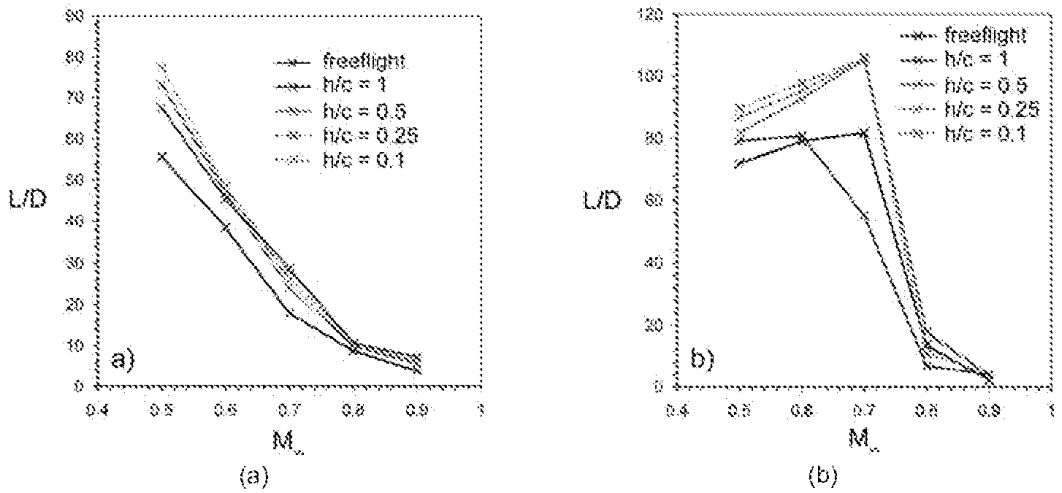

Figure 17. Aerodynamic efficiency, *L/D*, at (a) 2·79° and (b) 6° for different ground clearances as Mach number is increased.

naturally around the aerofoil without the constriction of the ground, at higher clearances. Clearly, the trim of an aircraft at low clearances accelerating or decelerating through the Mach number range would be continuously changing. This would occur abruptly in the case of lower shock formation, and would imply a necessity for rapid-response pitch correction to maintain altitude. Alternatively, any sudden change to altitude over the small ground clearance range would have significant effects for stability at a constant flight Mach number.

The aerodynamic efficiency of the aerofoil at the various ground clearances with increasing Mach number is shown in Fig. 17. The lower-surface-shock dominates the flowfield at h/c = 0·1 at M_∞ 0·6 onwards, with the immediate result being that it is considerably less efficient to fly at this ground clearance than in freeflight. The clearances of h/c = 0·25 represents the best efficiency gains until M_∞ 0·8, at which point the aerofoil at all clearances features a shock on the lower surface and thus lift drops off as drag increases. The peak efficiency for all clearances bar h/c = 0·1 comes at M_∞ 0·7, beyond which large-scale shock-induced separation destroys the advantages of flying in ground effect.

3.4.3 6° incidence

At the maximum incidence, the lift and drag behaviours are similar to those at 2·79°, with a peak in C_L occurring at M_∞ 0·7 for all cases from freeflight to h/c = 0·5. In freeflight the drop off in C_L is continuous thereafter, whereas at the higher ground clearances a partial recovery is made at M_∞ 0·9 as the 'ram' effect under the aerofoil continues and extensive separation on the upper surface of the wing is no longer possible with the shock waves now sitting at the trailing edge. The disappearance of the lower surface shock over these clearances serves to aid greatly in the recovery of lift. At h/c = 0·1, the drop in lift at M_∞ 0·8 is mild, such is the increase to effective angle of incidence at this clearance, and thus at this clearance the wing remains more efficient through the Mach range than in freeflight as shown in Fig. 16, although the large-scale separation it produces means that it is never more than a few percent more efficient than the lower-drag cases at higher ground clearances. The figure also highlights a clear trend towards decreasing efficiency with increasing Mach number (in ground effect as in freeflight), with the shock-separation induced drag the prime contributor to this.

4.0 CONCLUSIONS

An RAE 2822 aerofoil section at Reynolds numbers approximating flight conditions was examined for multiple ground clearances (freeflight (no ground), and h/c = 1, 0·5, 0·25, and 0·1), Mach numbers (0·5, 0·6, 0·7, 0·8, 0·9) and angles of incidence (0°, 2·79° and 6°).

In general, the ground effect mechanisms that result in increased lift and often enhanced efficiency at much lower Mach numbers also hold at high-subsonic Mach numbers. High pressure increases underneath the aerofoil as more mass flow is directed over the upper surface, leading to an increase in effective angle of incidence. This is rarely the case at very low clearances (h/c = 0·1), where the local curvature at the leading edge on the lower surface encourages the flow to accelerate under the section to create enough low pressure over the middle portion of the aerofoil to have a strong destructive effect on lift.

The onset of shock waves in the flowfield has a disruptive effect on performance, particularly at the lowest clearances, where the early formation of a shock wave between the aerofoil and ground can lead to a sudden drop in the production of lift and an accompanying early transonic drag rise for the section. It can also lead to the development of unsteady shock oscillations on

the lower surface, and has a considerable effect on the pitching moment of the section, lending it a nose-up moment at low clearances where it would normally have a nose-down moment at higher clearances and in freeflight.

While an aerofoil could be optimised to delay or mitigate many of the undesirable effects described, it remains clear that sustained flight close to the ground at transonic Mach numbers would be particularly difficult without an advanced control system to account for very rapid changes to lift, drag and pitching moment caused by relatively small changes to ground clearance, incidence or Mach number. For instance, if flying close to the critical Mach number for the lower surface at $h/c = 0{\cdot}1$, even a sudden strong headwind gust could result in the abrupt formation of a shock wave between the aerofoil and ground causing a precipitous loss in lift and therefore altitude.

The results indicate that without further research into appropriate aerofoil shapes and longitudinal control, a craft specifically designed to fly in ground effect at high subsonic Mach numbers is not a feasible prospect, and thus an 'upper limit' to the cruising Mach number of such a craft would apply. The aerodynamic efficiency of the section at different ground clearances for increasing Mach number indicated that the onset of supersonic flow on the lower surface, achieved as early as $M_\infty 0{\cdot}5$ at $h/c = 0{\cdot}1$, means that flight in close ground proximity is no longer more efficient than freeflight. At the higher clearances, a peak in L/D occurs at $M_\infty 0{\cdot}7$, beyond which there is little gain to be made by flying in ground effect, as increased separation and lower surface suction cancel out any enhanced effective angle of incidence.

ACKNOWLEDGEMENTS

The authors gratefully acknowledge the support of The Royal Aeronautical Society: collaboration between the University of New South Wales and the US Naval Academy was made possible thanks to the RAeS through a Centennial CAARC Award to the primary author.

REFERENCES

1. Barber T.J., Leonardi E. and Archer R.D. Causes for discrepancies in ground effect analyses, *Aeronaut J*, 2002, **106**, (1066), pp 653-657.
2. Ahmed, M.R. and Sharma, S.D. An investigation on the aerodynamics of a symmetrical airfoil in ground effect, *Experimental Thermal and Fluid Science*, 2005, **29**, pp 633--647.
3. Rozhdestvensky, K.V. Aerodynamics of a Lifting System in Extreme Ground Effect (text), 1st ed., Springer-Verlag, New York, USA, 2000.
4. Powell, J., Maise, G., Paniagua, J. and Rather, J. Maglev Launch and the Next Race to Space, IEEE Aerospace Conference Proceedings, 2008, Big Sky, USA.
5. Schetz, J.A. Aerodynamics of High Speed Trains, *Annual Review of Fluid Mechanics*, 2001, **33**, pp 371-414.
6. Rozhdestvensky, K.V. Wing-in-ground effect vehicles, *Progress in Aerospace Sciences*, 2006, **42**, (3), pp 211-283.
7. Maskalik, A.I. and Rozhdestvensky, K.V. A View of the Present State of Research in Aero- and Hydrodynamics of Ekranoplans, RTO AVT Symposium on Fluid Dynamics Problems of Vehicles Operating near or in the Air-Sea Interface, Amsterdam, The Netherlands, 5-8 October 1998.
8. Dragos, L. Numerical solutions of the equation for a thin airfoil in ground effect, 1990, *AIAA J*, **28**, (12), pp 2132-2134.
9. Dragos, L. and Dinu, A. A direct boundary integral equations method to subsonic flow with circulation past thin airfoils in ground effect, *Comput Methods Appl. Mech Eng*, 1995, **121**, pp 163-176.

10. COOK, P.H., MCDONALD, M.A. and FIRMIN, M.C.P. Aerofoil RAE 2822 - Pressure Distributions, and Boundary Layer and Wake Measurements. Experimental Data Base for Computer Program Assessment, 1979, AGARD Report AR 138.
11. DOIG, G.D., BARBER, T.J., NEELY, A.J. and MYRE, D.D. Aerodynamics of an Aerofoil in Transonic Ground Effect: Methods for Blowdown wind-tunnel Scale Testing. Submitted to *the Aeronautical Journal*, November 2010, revised May 2010.
12. Fluent User Guide, 2006, FLUENT Inc., Lebanon, NH.
13. SUTHERLAND, W. The viscosity of gases and molecular force, *Philosophical Magazine*, 1893, **5**, (36), pp 507-531.
14. GARBARUK, A., SHUR, M., STRELETS, M. and SPALART, P.R. Numerical study of wind-tunnel wall effects on transonic airfoil flow, *AIAA J.* 2003, **41**, (6), pp 1046-1054.
15. SUDANI, N., SATO, M., KANDA, H. and MATSUNO, K. Flow visualization studies on sidewall effects in two-dimensional transonic airfoil testing, *J Aircr*, 1994, **31**, (6), pp 1233-1239.
16. SPALART, P. and ALLMARAS, S. A one-equation turbulence model for aerodynamic flows, 1992, AIAA Paper 92-0439.
17. SHIH, T.H., LIOU, W.W., SHABBIR, A., YANG, Z. and ZHU, J. A new k-ε eddy-viscosity model for high Reynolds number turbulent flows -- model development and validation, 1995, *Computers & Fluids*, **24**, (3), pp 227-238.
18. MENTER, F.R. Two-equation eddy-viscosity turbulence models for engineering applications, *AIAA J*, 1994, **32**, 8, pp 269-289.
19. RUMSEY, C.L. and VATSA, V.N. A comparison of the predictive capabilities of several turbulence models using upwind and central-difference computer codes, 1993, Proc. 31st AIAA Aerospace Sciences Meeting, Reno, USA, pp 1-16.
20. SZWABA, R., DOERFFER, P., NAMIE, K. and SZULC, O. Flow structure in the region of three shock wave interaction, *Aerospace Science and Technology*, 2004, **8**, (6), pp 499-508.